






High- T_C ferromagnetic inverse Heusler alloys: A comparative study of Fe_2RhSi and Fe_2RhGe Y. Venkateswara ¹, S. Shanmukharao Samatham,^{1,2} Akhilesh Kumar Patel ¹, P. D. Babu ³, Manoj Raama Varma,⁴ K. G. Suresh ^{1,*} and Aftab Alam ^{5,†}¹Magnetic Materials Laboratory, Department of Physics, Indian Institute of Technology Bombay, Mumbai 400076, India²Department of Physics, Maharaj Vijayaram Gajapathi Raj College of Engineering, Vijayaram Nagar Campus, Chintalavalasa, Vizianagaram 535005, Andhra Pradesh, India³UGC-DAE Consortium for Scientific Research, Mumbai Centre, BARC Campus, Mumbai 400085, India⁴National Institute of Interdisciplinary Sciences and Technology (CSIR), Tiruvananthapuram 695019, India⁵Materials Modeling Laboratory, Department of Physics, Indian Institute of Technology Bombay, Mumbai 400076, India

(Received 24 February 2021; accepted 23 August 2021; published 1 September 2021)

We report the results of experimental investigations on structural, magnetic, resistivity, and caloric properties of Fe_2RhZ ($Z = \text{Si, Ge}$) along with *ab initio* band structure calculations using first-principle simulations. Both alloys are found to crystallize in inverse Heusler structure but with disorder in tetrahedral sites between Fe and Rh. Fe_2RhSi has a saturation moment of $5.00 \mu_B$ and while its counterpart has $5.19 \mu_B$. Resistivity measurement reveals a metallic nature in both of them. Theoretical simulations using generalized gradient approximation (GGA) predict an inverse Heusler structure with ferromagnetic ordering as a ground state for both alloys. However, it underestimates the experimentally observed moments. GGA+ U approach, with Hubbard U values estimated from density functional perturbation theory, helps to improve the comparison of the experimental results. Fe_2RhSi is found to be a half-metallic ferromagnet while Fe_2RhGe is not. Varying U values on Fe and Rh sites does not change the net moment much in Fe_2RhSi , unlike in Fe_2RhGe . Relatively small exchange splitting of orbitals in Fe_2RhGe compared to that of Fe_2RhSi is the reason for not opening the band gap in the minority spin channel in the former. High ordering temperature and moment make Fe_2RhSi useful for spintronics applications.

DOI: [10.1103/PhysRevB.104.094402](https://doi.org/10.1103/PhysRevB.104.094402)**I. INTRODUCTION**

Heusler alloys (HAs) [1] are well known due to their multifunctional properties such as (i) half-metallic ferromagnetism [2,3], spin gapless semiconducting nature [4–6], bipolar magnetic semiconductors [7], and spin semimetals [8]. (ii) High spin polarization. (iii) Superconductivity arising in the alloys containing 27 valence electrons such as Ni_2ZrGa [9], Pd_2RSn ($R = \text{Tb-Yb}$) [10–12], AuPdTM ($T = \text{Sc, Y}$ and $M = \text{Al, Ga, In}$) [13], etc. (iv) Giant exchange bias [14,15]. (v) Martensitic transition which causes large magnetocaloric effect (MCE) [16–18] and topological insulating behavior [19–25] and Weyl semimetals [26,27]. For the last three decades, after discovery of half-metallicity in NiMnSb by de Groot *et al.* [2], HAs gained prominence in the field of spintronics. Among the studied systems, Co-based Heusler alloys got increased attention due to their high Curie temperature (T_C). In addition to the $3d$ based HAs, $4d$ based alloys were also studied for spintronic applications. Some of the examples are $\text{Ru}_{2-x}\text{Fe}_x\text{CrGe}$ [28], $\text{Ru}_{2-x}\text{Fe}_x\text{CrSi}$ [29], Ru_2MnZ ($Z = \text{Si, Ge, Sn, and Sb}$) [30], $(\text{Ru}_{1-x}\text{Co}_x)_2\text{FeSi}$ [31], RuMn_2Z ($Z = \text{Si, Sn}$) [32], and CoFeRuZ ($Z = \text{Si, Ge}$) [33]. In these alloys, Ru couples antiferromagnetically with neighboring magnetic

ions. The other important high- T_C series of $4d$ based Heusler alloys are Rh based. There has been extensive effort in the synthesis of the class of Rh_2TX ($T = \text{Ti, V, Cr, Mn, Fe, Co, Ni, Cu}$; $X = \text{Al, Ga, Ge, Si, Sb, Pb}$) alloys [34–40]. However, $L2_1$ order is found only for $T = \text{Mn, Ni, and Cu}$. Others either show tetragonal distortion or involve multiphases. Interestingly, in almost all studies in the literature on Rh-based HAs, researchers have achieved the ordered $L2_1$ structure only if the total number of valence electrons of the alloy is odd. Some of the examples include Rh_2MnX ($X = \text{Ge, Sn, Pb}$) [34], Rh_2CuSn [36,41,42], LiRh_2X ($X = \text{Si, Ge}$) [43], CoRhMnSn [44], CoRhMnGe [45], FeRhCrGe [8], etc. Even though Rh_2NiGe is reported to crystallize in $L2_1$ structure, one can notice extra impurity peaks in the reported XRD data [38].

Rh-based Heusler alloys, with an even number of valence electrons, show tetragonal distortion which can be explained using band Jahn-Teller effect [46]. For these alloys, Coulomb repulsion also plays a crucial role in separating out the electronic states by broadening of the energy bands (close to the Fermi level), resulting in lattice distortion. One exception is the set of alloys containing Mn, such as CoRhMnGa [44], as Mn has the ability to adopt different oxidation states. Another reason is the nature of hybridization of the Mn atom with different neighboring orbitals as can be noticed in CoRuMnSi [47], unlike the general hybridization followed in other HAs reported elsewhere [48,49]. See the Supplementary Material [8] for more details.

*suresh@phy.iitb.ac.in

†aftab@phy.iitb.ac.in

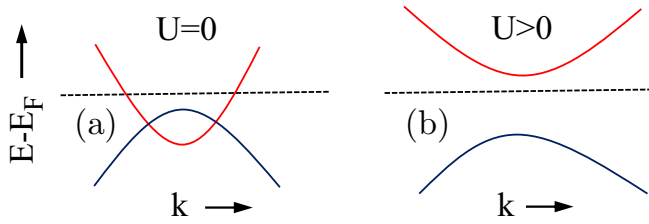


FIG. 1. Atom projected orbital character of bands close to Fermi level. (Left) Direct overlap of orbitals in the absence of Hubbard (U) correction. (Right) Gapped orbitals due to the inclusion of Hubbard correction. Partially occupied orbital (red color) corresponds to octahedral site while valence orbital (blue color) corresponds to tetrahedral sites in Heusler alloy.

In this paper we report two new odd-valence electron Rh-based full Heusler alloys Fe_2RhZ ($Z = \text{Si, Ge}$). A detailed experimental investigation involving structural, magnetic, and transport behavior is carried out. Additionally, first-principle calculations are done to better understand the magnetic ordering and the electronic structure.

Fe_2RhZ ($Z = \text{Si, Ge}$) are 29 valence electrons Heusler systems and hence are the analog of $3d$ -based Heusler alloys such as Fe_2CoSi [50], Fe_2CoGe [51,52], Co_2FeSi [53–56], Co_2FeGe [57–60], etc. Wurmehl *et al.* [54,56] and Uvarov *et al.* [58,59] studied Co_2FeSi and Co_2FeGe , respectively, and reported that they could only produce the experimentally observed moment and gap in the minority band by applying Hubbard U on these systems. But they have neither discussed why they have to include Hubbard U in their systems nor gave a clear indication to what type of Heusler systems should be included. There is an ambiguity of inclusion of U in all Heusler systems. Here we present a systematic way to observe and identify which Heusler systems need to be taken care with the inclusion of Hubbard correction. Figure 1(a) represents the atom resolved orbital character of band structure without Hubbard correction. If one notices such a direct overlap of orbitals (or slightly gapped) typically around the edges of the Brillouin zone (or away from the Γ point), they need to identify the atomic orbital character of these bands. (One can recall that the orbitals at Γ represent molecular levels of the corresponding system.) If the partially occupied conduction band [indicated by red color in Fig. 1(a)] arises from the octahedral site while the valence band arises from the tetrahedral site, then one should not neglect the Hubbard correction in the Heusler system. This kind of scenario generally occurs in high valence systems in the spin down band around X point in the Brillouin zone. As per the empirical rule stated in Ref. [61] for the formation of Heusler alloys based on electronegativities of constituent atoms, the octahedral sites try to lose partial electrons. Hence, the partially occupied conduction band which corresponds to the octahedral site lose their states by shifting their orbitals above the Fermi level. Such an observation can only be achieved by the inclusion of U in the system as shown in Fig. 1(b). Because U correction favors integer particle numbers in the system by penalizing the partial occupancies. Therefore one should look for such direct overlap of orbitals (i) in minority band for ferro, ferri, or fully compensated ferrimagnets or (ii) in the full band structure for

antiferromagnets or nonmagnetic systems. The effect of U is to open up the gap around the k point in the Brillouin zone but does not always guarantee the entire Brillouin zone as shown for Fe_2RhGe later in this paper. With this methodology one can predict very accurate results prior to experimental observations.

Theoretically, full Heusler alloys can accommodate a maximum of 31 valence electrons and can have a moment close to $7 \mu_B$. This happens only when the spin up bands are completely filled with an integral number of electrons. Experimentally, all such high valence electron systems reported in the literature belong to 29 and 30 valence electrons category. Fe_2RhZ ($Z = \text{Si, Ge}$) are the two new systems belonging to this category, with reasonably large T_C and magnetic moment.

II. EXPERIMENTAL TECHNIQUES

Both Fe_2RhSi and Fe_2RhGe alloys were prepared in polycrystalline form by the arc-melting method. Room temperature x-ray diffraction (XRD) patterns were collected by PANalytical X'Pert Pro powder diffractometer using $\text{Cu } K_\alpha$ radiation. Rietveld refinement of XRD patterns were analyzed using FullProf [62] package while VESTA [63] software is used for visualizing crystal structures. Magnetization measurements were carried out using Physical Property Measurement System (PPMS) model 6000 within the vibrating sample magnetometer (VSM) option. Temperature dependence of magnetization from 2 to 350 K is collected in different modes such as zero field cooling (ZFC) and field cooled cooling (FCC). High- T data collection was done in the high-temperature regime in which the sample is kept in the heating oven in the PPMS using the VSM option. Resistivity measurements were carried out using PPMS at different magnetic fields. Specific heat measurements were carried out from 2 to 280 K at zero field in PPMS using relaxation calorimetry.

III. COMPUTATIONAL DETAILS

Fe_2RhZ ($Z = \text{Si, Ge}$) with the stoichiometry 2:1:1 belong to the full Heusler alloy family. There exist two nondegenerate crystal configurations/structures in this class: (i) inverse Heusler structure (X type structure with prototype CuHg_2Ti , space group $F\bar{4}3m$) and (ii) normal Heusler structure ($L2_1$ structure with prototype Cu_2MnAl , space group $Fm\bar{3}m$) which are shown in Figs. 2(a) and 2(b), respectively. Since the valence of Fe is less than that of Rh, these alloys are expected to crystallize in the inverse Heusler structure. It originates from the simple empirical rule [48]. In a full HA X_2YZ , keeping Z at $4a$ site [i.e., at (0,0,0)], the lattice sites involving Fe and Rh atoms can have the following two configurations:

(1) Fe1 at $4b(\frac{1}{2}, \frac{1}{2}, \frac{1}{2})$, Fe2 at $4c(\frac{1}{4}, \frac{1}{4}, \frac{1}{4})$, and Rh at $4d(\frac{3}{4}, \frac{3}{4}, \frac{3}{4})$.

(2) Rh at $4b(\frac{1}{2}, \frac{1}{2}, \frac{1}{2})$ and Fe's at $4c(\frac{1}{4}, \frac{1}{4}, \frac{1}{4})$ and $4d(\frac{3}{4}, \frac{3}{4}, \frac{3}{4})$.

We used Quantum ESPRESSO [64,65] to simulate the two systems with different initial structural and spin configurations on Fe and Rh ions, and find the most stable (ground) state. Exchange correlations are incorporated within the generalized gradient approximation (GGA) and the

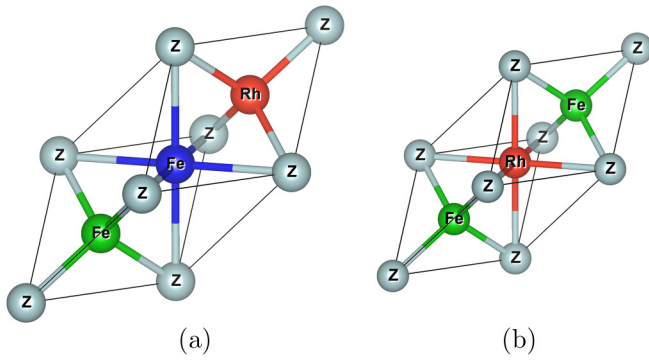


FIG. 2. Possible crystallographic configurations for Fe_2RhZ ($Z = \text{Si}, \text{Ge}$) full HAs. (a) Inverse Heusler structure (configuration I) and (b) normal Heusler structure (configuration II).

pseudopotentials parametrized by plane augmented wave method (KJPAW) [66] were generated using PSLibrary [67]. Other computational parameters used here are the same as in our previous report [68]. We used XCrySDen for making a k -point path for band structure calculations [69]. We have used Thermo-PW to simulate the electronic heat capacity of Fe_2RhZ ($Z = \text{Si}, \text{Ge}$) with temperature. In order to predict the effect of disorder on electronic and magnetic properties of alloys, we have used a Monte Carlo special quasirandom structure (MCSQS) as implemented in ATAT [70,71]. We have generated a disorder structure involving a 32 atoms supercell, as shown in Fig. 3.

IV. EXPERIMENTAL RESULTS

A. Crystal structure

Figures 4(a) and 4(c) show the room temperature XRD pattern along with their Rietveld refinement for Fe_2RhSi and Fe_2RhGe , respectively. The XRD pattern can be indexed with CuHg_2Ti type inverse Heusler structure with lattice parameters 5.77 and 5.88 Å for the two alloys, respectively. However, the observed peak intensity is weaker than that calculated for the odd superlattice reflections such as (111), (311), etc., indicating disorder between either tetrahedral site or octahedral site atoms. Octahedral disorder between Fe and Z(Si,Ge) does not fit well, whereas 50% disorder of tetrahedral site atoms

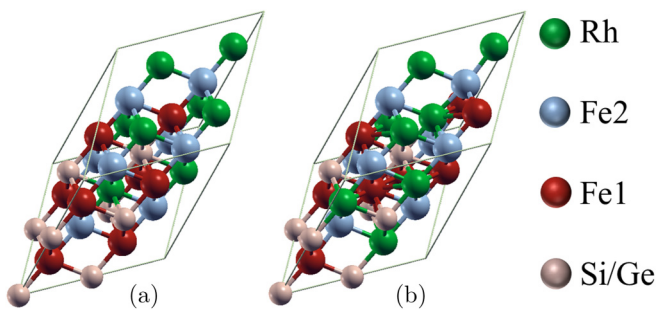


FIG. 3. Supercells of size $2 \times 2 \times 2$ for the inverse Heusler structure. (a) Having perfect inverse Heusler structure. (b) MCSQS having 50% disorder between tetrahedral sites Fe1 and Rh in Fe_2RhZ ($Z = \text{Si}, \text{Ge}$).

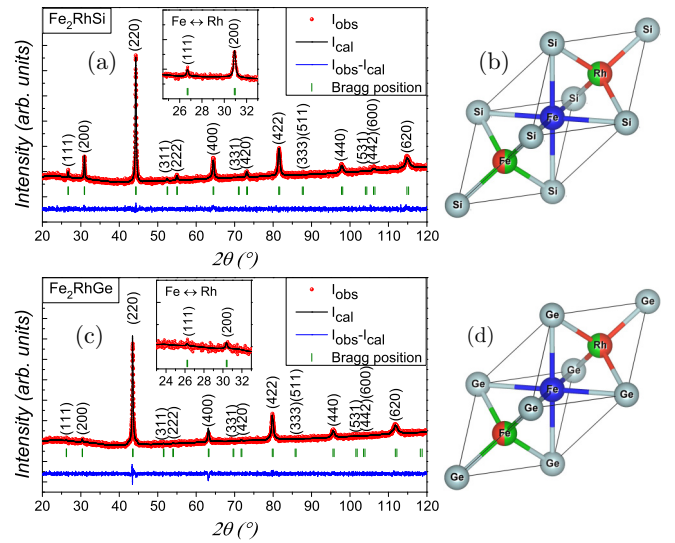


FIG. 4. Rietveld refinement of room temperature XRD data for (top) Fe_2RhSi and (bottom) Fe_2RhGe , respectively. Inset of (a) and (c) show the zoomed-in view of the refined data considering disorder between Fe and Rh in inverse Heusler structure (best fit). (b) and (d) Primitive cells corresponding to the best fit in (a) and (c), respectively.

Fe and Rh in configuration I fits very well [see the zoomed-in view of Figs. 4(a) and 4(c)]. Figures 4(b) and 4(d) show the primitive cells corresponding to the best fit. Refinement does not fit well for both odd and even superlattice reflection peaks in configuration II (Cu_2MnAl type structure). Moreover, any amount of disorder such as (i) $L2_1$ disorder between either octahedral or tetrahedral sites, (ii) DO_3 disorder, (iii) $B2$ disorder, and (iv) $A2$ disorder also did not fit well for configuration II. Hence, we conclude that both alloys crystallize in an inverse Heusler structure with 50% disorder between tetrahedral site atoms Fe and Rh.

B. Magnetization

The magnetization (M) in full Heusler alloys can be roughly estimated using the Slater-Pauling (SP) rule [49] given below:

$$M = (N_v - 24) \mu_B/\text{f.u.}, \quad (1)$$

where N_v is the total number of valence electrons in the alloy. Since both alloys have 29 valence electrons, they are expected to have a saturation moment of $5 \mu_B/\text{f.u.}$, as per SP rule.

Both alloys are found to be ferromagnetic in nature with high Curie temperatures. Magnetization vs field data at 3 and 300 K are shown in Figs. 5(a) and 5(c) for Fe_2RhSi and Fe_2RhGe , respectively. Fe_2RhSi has saturation moment of $5 \mu_B/\text{f.u.}$, whereas Fe_2RhGe has $5.19 \mu_B/\text{f.u.}$ Using the Arrott plots, we find that Fe_2RhSi has saturation moment of $4.98 \mu_B/\text{f.u.}$, whereas Fe_2RhGe has $5.22 \mu_B/\text{f.u.}$, which are consistent with the SP rule. Nearly integer moment on Fe_2RhSi indicates the possibility of half-metallic nature. Figures 5(b) and 5(d) show the temperature dependence of magnetization for the two alloys up to 1000 K at 10 kOe. The estimated T_C from magnetization data is found to be 940 and

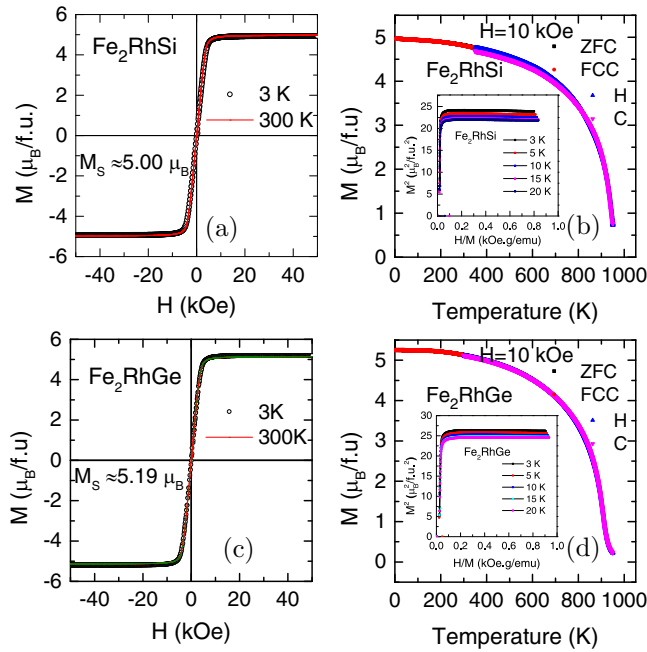


FIG. 5. (a) Magnetization vs field (H) at 3 and 300 K for (a) Fe_2RhSi and (c) Fe_2RhGe . Magnetization vs temperature (T) at 10 kOe for (b) Fe_2RhSi and (d) Fe_2RhGe . Insets of (b) and (d) show the Arrott plots for Fe_2RhSi and Fe_2RhGe , respectively.

910 K for Fe_2RhSi and Fe_2RhGe , respectively. Interestingly, these values are the highest in Heusler alloys containing at least one $4d$ or $5d$ transition element.

Though SP rule is respected by several full/half Heusler alloys, there are exceptions such as ferromagnetic/ferrimagnetic full Heusler alloys. Among these, only the spontaneous moment of half-metals follow the SP rule. Several ferromagnetic Heusler alloys are itinerant electron magnets, the magnetic properties of which are explained by spin-fluctuation theory.

C. Resistivity

Figure 6 shows the temperature dependence of resistivity for Fe_2RhSi and Fe_2RhGe , measured in the range 2–350 K. Measurements were carried out at different magnetic fields 0, 5, 10, and 50 kOe. In zero field, the positive temperature coefficient of $\rho(T)$ indicates metallic behavior. The

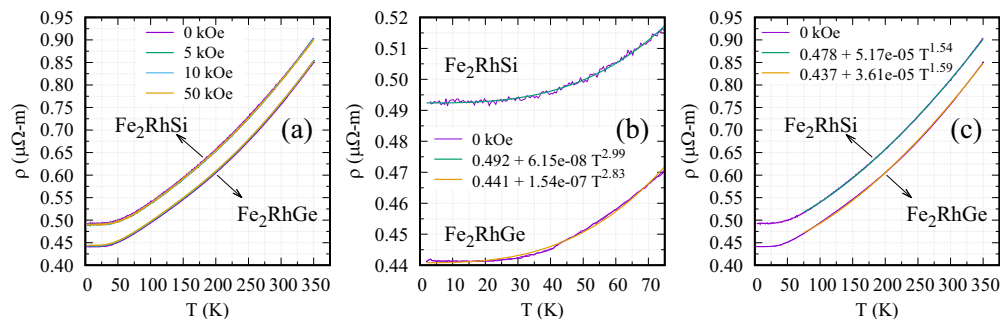


FIG. 6. (a) Temperature (T) dependence of resistivity (ρ) at different magnetic fields for Fe_2RhSi and Fe_2RhGe . (b) Low T and (c) high- T exponent fit [$\rho(T) = \rho_0 + AT^n$] to the resistivity data for Fe_2RhSi and Fe_2RhGe .

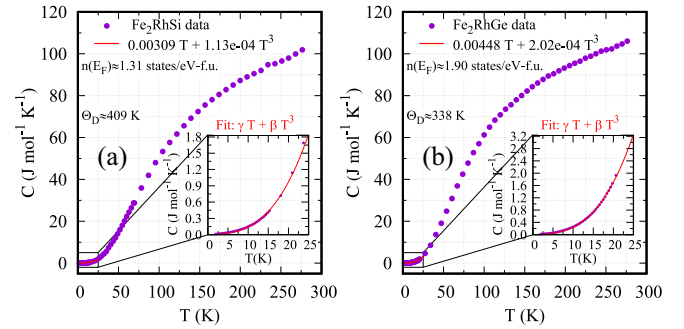


FIG. 7. Specific heat (C) vs T for (a) Fe_2RhSi and (b) Fe_2RhGe between 2–280 K in zero field. Insets show the zoomed in view of the low temperature fit $C(T) = \gamma T + \beta T^3$ in the T range 2–22 K.

application of field does not change the resistivity behavior much, as evident from Fig. 6(a), thereby indicating the robust magnetic ordering of the alloys. The absence of positive magnetoresistance indicates the marginal effect of field on the motion of conduction electrons. Resistivity data are fitted with the relation $\rho = \rho_0 + AT^n$ where ρ_0 is the residual resistivity. The residual resistance ratio ($\text{RRR} = R_{300\text{K}}/R_{2\text{K}}$) of Fe_2RhSi and Fe_2RhGe is ≈ 1.6 . Such a low RRR, as compared to that of conventional metals, is typical to Heusler alloys. Figures 6(b) and 6(c) show the fitted curve in two temperature regions (2–75 K and 50–350 K) with almost equal residual resistivity values. In the low T region, the exponents turn out be ~ 2.99 and ~ 2.83 for Fe_2RhSi and Fe_2RhGe , respectively, while they are $n \sim 1.54$ and ~ 1.59 in the high- T range. Furukawa derived the expression $\rho \propto (T/D_s)^3$ for the possible anomalous single magnon scattering at low temperatures in half-metals [72]. The same behavior is also observed in half-metallic systems $\text{Sm}_{0.6}\text{Sr}_{0.4}\text{MnO}_3$ and $(\text{Nd}_{0.8}\text{Tb}_{0.2})_{0.6}\text{Sr}_{0.4}\text{MnO}_3$ [73]. Hence the T^3 dependence observed in Fe_2RhSi at low temperatures indicates the half-metallic nature, whereas the exponent for Fe_2RhGe is slightly off from cubic dependence. The exponent in the high- T fitting, however, is close to $5/3$, indicating the presence of high temperature spin waves [74,75].

D. Specific heat

Figures 7(a) and 7(b) show the temperature dependence of zero field specific heat (C) for Fe_2RhSi and Fe_2RhGe , respectively. The low temperature specific heat is fitted to the expression $C(T) = \gamma T + \beta T^3$ from 2–22 K, as shown

TABLE I. Relaxed lattice parameter (a_0), atom projected moments and total cell moment, and relative energy (ΔE) of different configurations of Fe_2RhZ ($Z = \text{Si}, \text{Ge}$) within GGA functional.

Config.	Alloy	a_0 (Å)	Moment (μ_B)				ΔE (meV/atom)
			4d	4b	4c	Total	
I	Fe_2RhSi	5.79	Fe ₁	Fe ₂	Rh	4.90	0.0
			1.70	2.80	0.40		
	Fe_2RhGe	5.90	1.84	2.84	0.35	5.03	0.0
II	Fe_2RhSi	5.80	Fe ₁	Rh	Fe ₂	4.38	282
			1.89	0.60	1.89		
	Fe_2RhGe	5.91	2.10	0.62	2.10	4.92	235

in the insets of Figs. 7(a) and 7(b), respectively. Here γT and βT^3 are electronic and low temperature phonon contributions. The density of states (DOS) at the Fermi level $n(E_F)$ responsible for electronic contribution is estimated using the relation $n(E_F) = 3\gamma/(\pi k_B)^2$ [76], where γ is the Sommerfeld constant obtained from the fit and k_B is the Boltzmann constant. The Debye temperature Θ_D is estimated using the relation $\Theta_D = \sqrt[3]{1944p/\beta}$, where β is the coefficient of T^3 dependence at low temperatures and p is the number of atoms in a formula unit. The values of γ and β in units of $\text{mJ mol}^{-1} \text{K}^{-2}$ and $\text{J mol}^{-1} \text{K}^{-4}$ are estimated to be 3.09 ± 0.33 and $(1.13 \pm 0.01) \times 10^{-4}$ for Fe_2RhSi and 4.48 ± 0.49 and $(2.02 \pm 0.02) \times 10^{-4}$ for Fe_2RhGe . Thus estimated $n(E_F)$ are 1.31 ± 0.13 and 1.90 ± 0.21 states/eV f.u. for Fe_2RhSi and Fe_2RhGe , respectively. The estimated Θ_D are 409 and 338 K for Fe_2RhSi and Fe_2RhGe , respectively. The estimated $n(E_F)$ values are in good agreement with the simulated results using GGA+ U approach. It predicts nearly 1.0 and 1.9 states/eV f.u. for Fe_2RhSi and Fe_2RhGe , respectively. The simulated electronic heat capacity at constant volume (C_V^{ele}) with temperature using Therom-PW for Fe_2RhZ ($Z = \text{Si}, \text{Ge}$) without any Hubbard U and with Hubbard U values from Table II are shown in Fig. S12 in the Supplemental Material. The simulated γ values for Fe_2RhSi and Fe_2RhGe with Hubbard U are 0.0028 and 0.0042 J/mol K^2 , which are in very good agreement with the experimental heat capacity. Whereas the simulated γ values without any Hubbard U are slightly

TABLE II. Self-consistently converged Hubbard energies (U) on Fe1, Fe2, and Rh atoms for the two configurations (I and II) of Fe_2RhZ ($Z = \text{Si}, \text{Ge}$).

Config.	Alloy	Hubbard U (eV)		
		4d	4b	4c
I	Fe_2RhSi	Fe1	Fe2	Rh
		5.2	4.1	6.8
	Fe_2RhGe	4.6	3.9	6.6
II	Fe_2RhSi	Fe ₁	Rh	Fe ₂
		3.8	5.3	3.8
	Fe_2RhGe	3.5	5.2	3.5

higher. The experimental values of C slightly larger than 100 $\text{J mol}^{-1} \text{K}^{-1}$ (Dulong-petit law) for $T > 250$ K indicate the presence of small but non-negligible magnon contribution to specific heat.

V. THEORETICAL RESULTS AND DISCUSSION

Both Fe_2RhSi and Fe_2RhGe alloys were fully relaxed in the two configurations I and II using a GGA functional. The magnetic state and their total energies at the relaxed lattice parameters (a_0) are listed in Table I. Configuration I is found to be energetically more stable indicating that the alloys prefer inverse Heusler structure. The calculated net magnetic moments for Fe_2RhSi and Fe_2RhGe are 4.90 and 5.03 μ_B , respectively, which are in fair agreement with the SP rule and the experimental values.

Figure 8 shows the spin resolved band structure and density of states for configuration I of Fe_2RhZ ($Z = \text{Si}$ and Ge) using the GGA functional. The band structure clearly indicates that neither of the two systems is half-metallic due to the presence of small finite DOS at E_F in the spin down band. The small DOS arises due to the overlap of pair of valence and conduction bands around X point in the Brillouin zone. The character of these bands is obtained by projecting atomic orbitals on different atomic sites, as shown in Fig. 9 for Fe_2RhSi . One can notice from Figs. 9(a)–9(c) that the conduction orbital is mainly contributed by the e_g character of the octahedral site Fe (denoted as Fe2) while the valence orbital by the t_{2g} character of the tetrahedral site Fe (denoted as Fe1) around the X point, as highlighted by dotted encircle. This depicts the Hubbard picture as these orbitals are arising from different sites, but by the same atom (i.e., Fe) and are overlapping with the same moment and energy due to direct overlap. This leaves the possibility of exchange of indistinguishable particles between two distinct sites of Fe. A similar scenario can be noticed in the band structure of Fe_2RhGe using the GGA functional (please see the Supplemental Material [77]). Hence, we decided to carry out the simulations using the GGA+ U functional. This is carried out in two ways: (i) self-consistent evaluation of U values on Hubbard atoms, i.e., Fe1, Fe2, and Rh, unlike the trial and error method, and (ii) stepwise increment of U on Hubbard atoms.

Self-consistent estimation of U values on different atomic sites (Fe1, Fe2, and Rh) in both configurations of Fe_2RhSi and Fe_2RhGe is carried out using the linear response method as described by Coccioni *et al.* [78]. (Please see the Supplemental Material [77] for details on deriving U values at different Hubbard sites.) U values are estimated with increasing supercell size and the converged values are taken for the final GGA+ U calculations.

Table II shows the converged Hubbard U energies on different atoms for both configurations of the two systems. One can notice the different U values on Fe1 and Fe2 due to their different chemical environments with $U_{\text{Fe1}} > U_{\text{Fe2}}$ for configuration I. In the second configuration, both Fe1 and Fe2 occupy the tetrahedral sites, and even if they are treated differently in our simulations, their U values came out to be the same as their chemical environments are identical. The U value on Rh decreases from the tetrahedral site (as in configuration I) to the octahedral site (in configuration II). Slightly

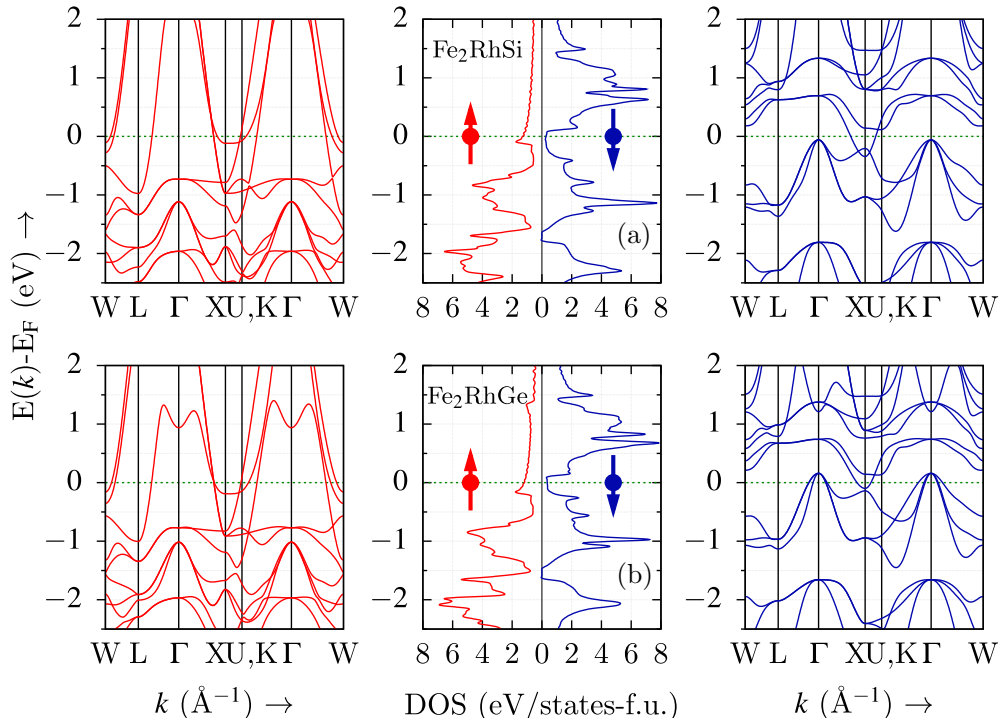


FIG. 8. Spin resolved band structure and density of states for configuration I of (top) Fe_2RhSi and (bottom) Fe_2RhGe at their equilibrium lattice parameter (a_0) within the GGA functional.

lower U values observed in Fe_2RhGe as compared to Fe_2RhSi can be attributed to the reduced hybridization strength due to the ligand atom (i.e., Si or Ge) (stronger hybridization leads to larger band splittings as seen in Fe_2RhSi).

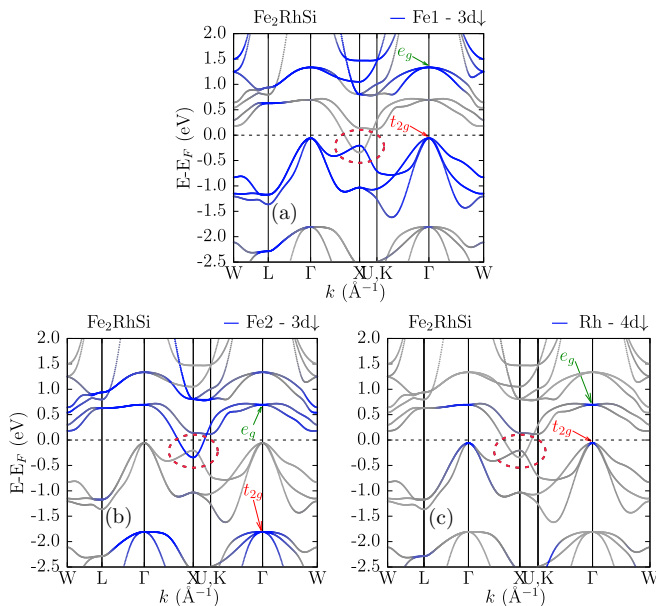


FIG. 9. d orbital projected band structure of spin down channel for configuration I of Fe_2RhSi with the GGA functional. (a) $3d$ orbital character of tetrahedral site atom Fe, (b) $3d$ orbital character of octahedral site atom Fe, and (c) $4d$ orbital character of another tetrahedral site atom Rh.

Looking at the U values on Rh (>6.6 eV) and Fe1 and Fe2 (>3.9 eV) for configuration I of Fe_2RhZ ($Z = \text{Si}, \text{Ge}$), one may argue that the estimated values are relatively large. However, these U values are comparable to those of a similar, large moment system Co_2FeSi [54]. This system has 30 valence electrons and hence carries a net moment of $6 \mu_B$ according to the SP rule. Wurmehl *et al.* reported it to be a ferromagnet with $T_C \approx 1100$ K and an experimental moment of $6 \mu_B$ [54]. It was reported that the experimentally observed moment can only be reproduced by the application of U in excess of 7.5 eV [3]. They also reported that the application of $U_{\text{eff}} = U - J$ (where J is the exchange parameter) ranging between 2.5 and 5.0 eV on the Co atom and (simultaneously) 2.4 to 4.8 eV on the Fe atom result in a moment of $6 \mu_B$ and a gap in the minority state [54]. $3d$ transition elements Fe and Ni are reported to have U values greater than 4.5 eV in FeO and NiO [78]. Therefore, the listed U values in Table II are within the expected range, for the considered elements.

Using the estimated U values from the linear response method (as tabulated in Table II) in the GGA+ U scheme [78], electronic/magnetic properties of configurations I and II of Fe_2RhZ ($Z = \text{Si}, \text{Ge}$) were investigated. Configuration I turns out to be energetically more stable in both cases. Figure 10 shows the spin resolved band structure and density of states for configuration I of Fe_2RhZ ($Z = \text{Ge}, \text{Si}$). Interestingly, Fe_2RhSi becomes a half-metal, whereas Fe_2RhGe remains metallic. The direct overlap of e_g conduction orbital and t_{2g} valence orbital around X point within GGA only approach (without U) are now separated out (see the dotted encircled region in Fig. 10) due to Hubbard energies. This also changes the partially occupied conduction e_g orbitals to fully

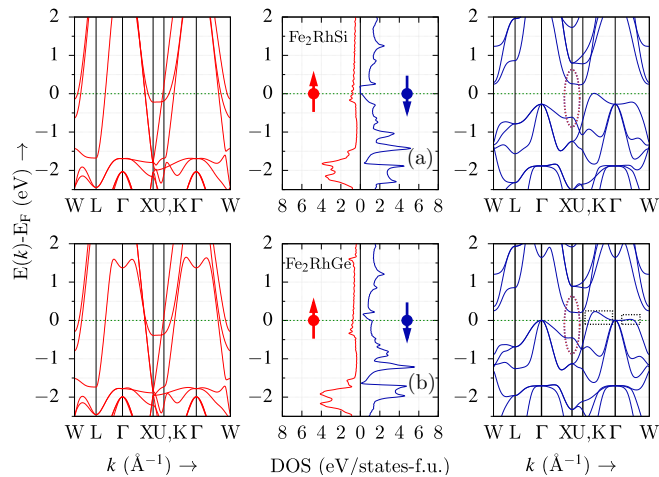


FIG. 10. Spin resolved band structure and density of states for (top) Fe_2RhSi and (bottom) Fe_2RhGe alloys using GGA+ U approach [78]. The U values used in this calculation are listed in Table II. Dotted encircle shows the location of the opening of gap. Dotted rectangle shows the location of hole pockets.

unoccupied ones by shifting them above the Fermi level in Fe_2RhZ ($Z = \text{Si, Ge}$). Fe_2RhGe does not become half metal even after applying U values because of lower band splitting energies and the presence of hole pockets in its spin down band structure. This is true even if one varies U values (on Fe1, Fe2, and Rh) in any range. On the other hand, Fe_2RhSi turns to be a half-metal for any U values above 1.0 eV on Fe1, Fe2, and Rh. One can notice the hole pockets along the paths Γ - K and Γ - W in the spin down band structure of Fe_2RhGe (see Fig. 10). These hole pockets are responsible not only for causing large total density of states at Fermi level, as evident from experimental specific heat analysis, but also for the high temperature single magnon scattering observed in resistivity analysis. The origin of the high temperature single magnon contribution to resistivity, observed for Fe_2RhSi , might be due to the presence of holelike bands touching the Fermi level in a spin down band structure (see Fig. 10). This approach predicts an almost constant moment of $5.00 \mu_B$ for Fe_2RhSi , unlike for Fe_2RhGe where the moment varies from 5.03 to $5.25 \mu_B$ as the U values increase.

The crystal structures which are simulated so far are still ordered in nature, however experiment confirms the formation of a slightly different structure with disorder at the tetrahedral sites (involving Rh and Fe1 atoms). In order to simulate the experimentally predicted structure, we have used the MCSQS simulation suite [70,71] to generate a 32 atom disordered supercell, as shown in Fig. 3. This is a fully relaxed structure with the same cutoff parameters and convergence as that used for primitive cell simulations. Figure 11 shows the spin resolved density of states and band structure for this disordered structure of Fe_2RhSi and Fe_2RhGe , including the effect of Hubbard U . One can notice that Fe_2RhSi still retains half-metallic character, whereas Fe_2RhGe shows a ferromagnetic metal. It predicts a net moment of 5.00 and $5.16 \mu_B/\text{f.u.}$ for Fe_2RhSi and Fe_2RhGe , respectively. The half-metallic band gap (for spin down channel) of Fe_2RhSi increases slightly with increasing U values, keeping the moment

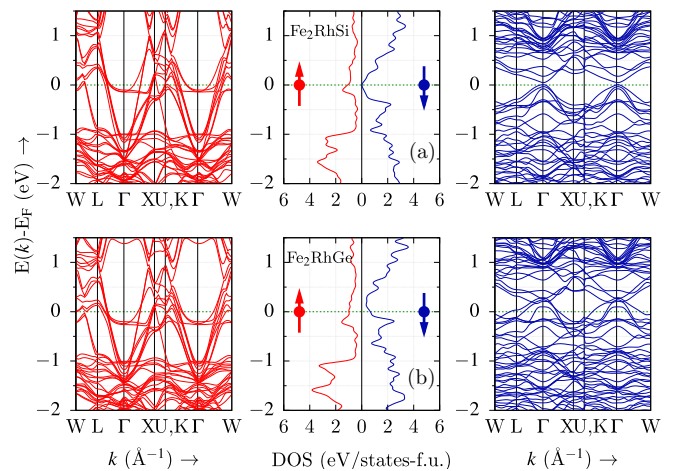


FIG. 11. Spin resolved density of states and band structure of disordered Fe_2RhZ ($Z = \text{Si, Ge}$) with tetrahedra site disorder (involving Rh and Fe_1 atoms).

almost constant. Fe_2RhGe still remains a ferromagnetic metal with increasing U values. One can argue that the 32 atom cell is not large enough to fully capture the disordered correlation. We have checked a couple of larger sized disordered cell as well, but the predictions related to half-metal vs metal remains intact.

VI. CONCLUSION

Fe_2RhZ ($Z = \text{Si, Ge}$) were synthesized experimentally and found to crystallize in an inverse Heusler structure. Both alloys are found to be ferromagnets with saturation magnetization 5.00 and $5.19 \mu_B$, respectively. These alloys have the highest T_C from the family of Heusler alloys having at least one $4d$ or $5d$ transition element. Resistivity measurement reveals a metallic nature for both systems. Integer moment and the presence of anomalous single magnon contribution to low temperature resistivity in Fe_2RhSi indicate the possibility of being a half-metal. Heat capacity analysis predicts larger density of states at Fermi level for Fe_2RhGe as compared to Fe_2RhSi and are in good agreement with the simulated values obtained using the GGA+ U functional. γ values from the simulated electronic heat capacity are also in very good agreement with the experimental values if one considers the GGA+ U functional. *Ab initio* calculations using the GGA approach predicts inverse Heusler structure with ferromagnetic ordering to be energetically more favorable. The band structure obtained with GGA calculations suggest metallic behavior for both alloys. In contrast, GGA+ U approach (with self-consistently calculated U values) opens up a gap at/around X point for the directly overlapped conduction e_g orbital and a valence t_{2g} orbital in spin down band structure for both systems. Interestingly it predicts a net moment of $5.00 \mu_B$ with a half-metallic nature for Fe_2RhSi . Fe_2RhGe , however, does not become half-metal because of relatively low band splitting energies (as compared to Fe_2RhSi) arising out of a weak hybridization and the presence of hole pockets along Γ - K and Γ - W path in the spin down band structure. Irrespective of U values (above 1.0 eV on Fe1, Fe2, and Rh) and the

nature of functionals (either LDA+ U or GGA+ U), Fe₂RhSi is found to be a half-metal while Fe₂RhGe remains metallic. MCSQS having 50% tetrahedral site disorder predicts Fe₂RhSi to be a half-metal, whereas Fe₂RhGe still shows a ferromagnetic metallic behavior within GGA+ U calculations. The effect of disorder as observed in the refinement can only be able to reduce the half-metal band gap but not its half-metal character. Simulated results based on the GGA+ U approach gives a very good overall agreement with experiment. As such, Fe₂RhSi can be a potential material for spintronics

application due to its high transition temperature, half-metallic nature, and higher crystal stability.

ACKNOWLEDGMENTS

Y.V. and S.S.S. acknowledge the financial support provided by IIT Bombay. Y.V. acknowledges Dr. D. Singh for his assistance in experimental measurements. A.A. acknowledges DST-SERB (Grant No. CRG/2019/002050) for funding to support this research.

-
- [1] F. Heusler, *Verhandlungen der Deutschen Physikalischen 2 Gesellschaft* (Friedr. Vieweg & Sohn, German, 1903), p. 219.
- [2] R. A. de Groot, F. M. Mueller, P. G. van Engen, and K. H. J. Buschow, *Phys. Rev. Lett.* **50**, 2024 (1983).
- [3] M. I. Katsnelson, V. Y. Irkhin, L. Chioncel, A. I. Lichtenstein, and R. A. de Groot, *Rev. Mod. Phys.* **80**, 315 (2008).
- [4] X. L. Wang, *Phys. Rev. Lett.* **100**, 156404 (2008).
- [5] Z. Yue, Z. Li, L. Sang, and X. Wang, *Small* **16**, 1905155 (2020).
- [6] X. Wang, Z. Cheng, J. Wang, X.-L. Wang, and G. Liu, *J. Mater. Chem. C* **4**, 7176 (2016).
- [7] X. Li, X. Wu, Z. Li, J. Yang, and J. G. Hou, *Nanoscale* **4**, 5680 (2012).
- [8] Y. Venkateswara, S. S. Samatham, P. D. Babu, K. G. Suresh, and A. Alam, *Phys. Rev. B* **100**, 180404(R) (2019).
- [9] J. Winterlik, G. H. Fecher, C. Felser, M. Jourdan, K. Grube, F. Hardy, H. von Löhneysen, K. L. Holman, and R. J. Cava, *Phys. Rev. B* **78**, 184506 (2008).
- [10] S. K. Malik, A. M. Umarji, and G. K. Shenoy, *Phys. Rev. B* **31**, 6971 (1985).
- [11] S. K. Malik, A. M. Umarji, and G. K. Shenoy, *Phys. Rev. B* **34**, 3144 (1986).
- [12] T. Klimczuk, C. H. Wang, K. Gofryk, F. Ronning, J. Winterlik, G. H. Fecher, J.-C. Griveau, E. Colineau, C. Felser, J. D. Thompson, D. J. Safarik, and R. J. Cava, *Phys. Rev. B* **85**, 174505 (2012).
- [13] L. Kautzsch, F. Mende, G. H. Fecher, J. Winterlik, and C. Felser, *Materials (Basel, Switzerland)* **12**, 2580 (2019).
- [14] A. K. Nayak, M. Nicklas, S. Chadov, P. Khuntia, C. Shekhar, A. Kalache, M. Baenitz, Y. Skourski, V. K. Guduru, A. Puri, U. Zeitler, J. M. D. Coey, and C. Felser, *Nat. Mater.* **14**, 679 (2015).
- [15] J. Sharma and K. G. Suresh, *Appl. Phys. Lett.* **106**, 072405 (2015).
- [16] I. D. Rodionov, Y. S. Koshkid'ko, J. Cwik, A. Quetz, S. Pandey, A. Aryala, I. S. Dubenko, S. Stadler, N. Ali, I. S. Titov, M. Blinov, V. N. Prudnikov, E. Lahderanta, I. Zakharchuk, and A. B. Granovsky, *Phys. Proc.* **75**, 1353 (2015), 20th International Conference on Magnetism, ICM 2015.
- [17] J. Liu, X. You, B. Huang, I. Batashev, M. Maschek, Y. Gong, X. Miao, F. Xu, N. van Dijk, and E. Brück, *Phys. Rev. Materials* **3**, 084409 (2019).
- [18] A. K. Nayak, K. G. Suresh, and A. K. Nigam, *J. Phys. D* **42**, 035009 (2009).
- [19] H. Yang, J. Yu, S. S. P. Parkin, C. Felser, C.-X. Liu, and B. Yan, *Phys. Rev. Lett.* **119**, 136401 (2017).
- [20] C. Li, J. S. Lian, and Q. Jiang, *Phys. Rev. B* **83**, 235125 (2011).
- [21] A. Pham and S. Li, *Phys. Rev. B* **95**, 115124 (2017).
- [22] C. K. Barman and A. Alam, *Phys. Rev. B* **97**, 075302 (2018).
- [23] W. Xiao-Tian, D. Xue-Fang, J. Hong-Ying, W. Li-Ying, L. Ran, L. Yong, L. Xiao-Chuang, Z. Xiao-Ming, W. Wen-Hong, W. Guang-Heng, and L. Liu Guo-Dong, *Acta Phys. Sin.* **63**, 023101 (2014).
- [24] S.-Y. Lin, M. Chen, X.-B. Yang, Y.-J. Zhao, S.-C. Wu, C. Felser, and B. Yan, *Phys. Rev. B* **91**, 094107 (2015).
- [25] B. Yan and A. de Visser, *MRS Bull.* **39**, 859 (2014).
- [26] K. Manna, Y. Sun, L. Muechler, J. Kübler, and C. Felser, *Nat. Rev. Mater.* **3**, 244 (2018).
- [27] Z. Wang, M. G. Vergniory, S. Kushwaha, M. Hirschberger, E. V. Chulkov, A. Ernst, N. P. Ong, R. J. Cava, and B. A. Bernevig, *Phys. Rev. Lett.* **117**, 236401 (2016).
- [28] P. J. Brown, A. P. Gandy, T. Kanomata, Y. Kusakari, A. Sheikh, K.-U. Neumann, B. Ouladdiaf, and K. R. A. Ziebeck, *J. Phys.: Condens. Matter* **20**, 455201 (2008).
- [29] I. Shigeta, O. Murayama, T. Hisamatsu, A. Brinkman, A. A. Golubov, Y. Tanaka, M. Ito, H. Hilgenkamp, and M. Hiroi, *J. Phys. Chem. Solids* **72**, 604 (2011), spectroscopies in Novel Superconductors 2010.
- [30] T. Kanomata, M. Kikuchi, H. Yamauci, and T. Kaneko, *Jpn. J. Appl. Phys.* **32**, 292 (1993).
- [31] B. Deka and A. Srinivasan, *Phys. B: Condens. Matter* **476**, 118 (2015).
- [32] K. Endo, T. Kanomata, H. Nishihara, and K. Ziebeck, *J. Alloys Compd.* **510**, 1 (2012).
- [33] L. Bainsla, M. M. Raja, A. Nigam, and K. Suresh, *J. Alloys Compd.* **651**, 631 (2015).
- [34] J. C. Suits, *Phys. Rev. B* **14**, 4131 (1976).
- [35] P. Klaer, M. Kallmayer, H. J. Elmers, L. Basit, J. Thöne, S. Chadov, and C. Felser, *J. Phys. D* **42**, 084001 (2009).
- [36] M. Yin and P. Nash, *J. Alloys Compd.* **650**, 925 (2015).
- [37] M. Pugacheva and A. Jezierski, *J. Magn. Magn. Mater.* **151**, 202 (1995).
- [38] T. Kanomata, Y. Adachi, H. Nishihara, H. Fukumoto, H. Yanagihashi, O. Nashima, and H. Morita, *J. Alloys Compd.* **417**, 18 (2006).
- [39] S. Berri, D. Maouche, M. Ibrir, F. Zerarga, L. Louail, and Y. Medkour, *Phys. B: Condens. Matter* **418**, 58 (2013).
- [40] M. Emmel and G. Jakob, *J. Magn. Magn. Mater.* **381**, 360 (2015).
- [41] K. Nikolaev, P. Kolbo, T. Pokhil, X. Peng, Y. Chen, T. Ambrose, and O. Mryasov, *Appl. Phys. Lett.* **94**, 222501 (2009).
- [42] R. Knut, P. Svedlindh, O. Mryasov, K. Gunnarsson, P. Warnicke, D. A. Arena, M. Björck, A. J. C. Dennison, A. Sahoo,

- S. Mukherjee, D. D. Sarma, S. Granroth, M. Gorgoi, and O. Karis, *Phys. Rev. B* **88**, 134407 (2013).
- [43] M. S. Bailey, Q. Li, E. B. Lobkovsky, D. Hinks, and J. Mitchell, *J. Solid State Chem.* **181**, 30 (2008).
- [44] V. Alijani, J. Winterlik, G. H. Fecher, S. S. Naghavi, S. Chadov, T. Gruhn, and C. Felser, *J. Phys.: Condens. Matter* **24**, 046001 (2012).
- [45] D. Rani, Enamullah, K. G. Suresh, A. K. Yadav, S. N. Jha, D. Bhattacharyya, M. R. Varma, and A. Alam, *Phys. Rev. B* **96**, 184404 (2017).
- [46] J. Suits, *Solid State Commun.* **18**, 423 (1976).
- [47] Y. Venkateswara, D. Rani, K. Suresh, and A. Alam, *J. Magn. Mater.* **502**, 166536 (2020).
- [48] T. Graf, C. Felser, and S. S. Parkin, *Prog. Solid State Chem.* **39**, 1 (2011).
- [49] I. Galanakis, P. H. Dederichs, and N. Papanikolaou, *Phys. Rev. B* **66**, 174429 (2002).
- [50] H. Luo, Z. Zhu, L. Ma, S. Xu, H. Liu, J. Qu, Y. Li, and G. Wu, *J. Phys. D* **40**, 7121 (2007).
- [51] Z. Ren, S. Li, and H. Luo, *Phys. B: Condens. Matter* **405**, 2840 (2010).
- [52] T. Gasi, V. Ksenofontov, J. Kiss, S. Chadov, A. K. Nayak, M. Nicklas, J. Winterlik, M. Schwall, P. Klaer, P. Adler, and C. Felser, *Phys. Rev. B* **87**, 064411 (2013).
- [53] S. Wurmehl, G. H. Fecher, H. C. Kandpal, V. Ksenofontov, C. Felser, and H.-J. Lin, *Appl. Phys. Lett.* **88**, 032503 (2006).
- [54] S. Wurmehl, G. H. Fecher, H. C. Kandpal, V. Ksenofontov, C. Felser, H.-J. Lin, and J. Morais, *Phys. Rev. B* **72**, 184434 (2005).
- [55] M. Sargolzaei, M. Richter, K. Koepf, I. Opahle, H. Eschrig, and I. Chaplygin, *Phys. Rev. B* **74**, 224410 (2006).
- [56] B. Balke, S. Wurmehl, G. H. Fecher, C. Felser, and J. Kübler, *Sci. Technol. Adv. Mater.* **9**, 014102 (2008).
- [57] M. Kim, H. Lim, and J. I. Lee, *Thin Solid Films* **519**, 8419 (2011), first International Conference of the Asian Union of Magnetism Societies (ICAUMS 2010).
- [58] N. V. Uvarov, Y. V. Kudryavtsev, A. F. Kravets, A. Y. Vovk, R. P. Borges, M. Godinho, and V. Korenivski, *J. Appl. Phys.* **112**, 063909 (2012).
- [59] D. Rai, A. Shankar, Sandeep, M. Ghimire, and R. Thapa, *Phys. B: Condens. Matter* **407**, 3689 (2012).
- [60] J.-M. Hyun and M. Kim, *J. Korean Phys. Soc.* **72**, 276 (2018).
- [61] Enamullah, Y. Venkateswara, S. Gupta, M. R. Varma, P. Singh, K. G. Suresh, and A. Alam, *Phys. Rev. B* **92**, 224413 (2015).
- [62] J. Rodríguez-Carvajal, *Phys. B: Condens. Matter* **192**, 55 (1993).
- [63] K. Momma and F. Izumi, *J. Appl. Crystallogr.* **44**, 1272 (2011).
- [64] P. Giannozzi, O. Andreussi, T. Brumme, O. Bunau, M. B. Nardelli, M. Calandra, R. Car, C. Cavazzoni, D. Ceresoli, M. Cococcioni, N. Colonna, I. Carnimeo, A. D. Corso, S. de Gironcoli, P. Delugas, R. A. D. Jr, A. Ferretti, A. Floris, G. Fratesi, G. Fugallo *et al.*, *J. Phys.: Condens. Matter* **29**, 465901 (2017).
- [65] P. Giannozzi, S. Baroni, N. Bonini, M. Calandra, R. Car, C. Cavazzoni, D. Ceresoli, G. L. Chiarotti, M. Cococcioni, I. Dabo, A. Dal Corso, S. de Gironcoli, S. Fabris, G. Fratesi, R. Gebauer, U. Gerstmann, C. Gougoussis, A. Kokalj, M. Lazzeri, L. Martin-Samos *et al.*, *J. Phys.: Condens. Matter* **21**, 395502 (2009).
- [66] G. Kresse and D. Joubert, *Phys. Rev. B* **59**, 1758 (1999).
- [67] A. Dal Corso, *Comput. Mater. Sci.* **95**, 337 (2014).
- [68] Y. Venkateswara, S. Gupta, S. S. Samatham, M. R. Varma, Enamullah, K. G. Suresh, and A. Alam, *Phys. Rev. B* **97**, 054407 (2018).
- [69] A. Kokalj, *J. Mol. Graphics Model.* **17**, 176 (1999).
- [70] A. van de Walle, M. D. Asta, and G. Ceder, *Calphad* **26**, 539 (2002).
- [71] A. van de Walle, P. Tiwary, M. M. de Jong, D. L. Olmsted, M. D. Asta, A. Dick, D. Shin, Y. Wang, L.-Q. Chen, and Z.-K. Liu, *Calphad* **42**, 13 (2013).
- [72] N. Furukawa, *J. Phys. Soc. Jpn.* **69**, 1954 (2000).
- [73] T. Akimoto, Y. Moritomo, A. Nakamura, and N. Furukawa, *Phys. Rev. Lett.* **85**, 3914 (2000).
- [74] K. Ueda and T. Moriya, *J. Phys. Soc. Jpn.* **39**, 605 (1975).
- [75] M. A. Kouacou, A. A. Koua, Z. Yeo, A. Akichi, A. Tanoh, and M. Koffi, *J. Appl. Sci.* **8**, 682 (2008).
- [76] C. W. Tseng, C. N. Kuo, H. W. Lee, K. F. Chen, R. C. Huang, C.-M. Wei, Y. K. Kuo, and C. S. Lue, *Phys. Rev. B* **96**, 125106 (2017).
- [77] See Supplemental Material at <http://link.aps.org/supplemental/10.1103/PhysRevB.104.094402> for further results on atom/orbital projected band structures, estimating Hubbard U values using linear response method, additional data based on LDA+ U and GGA+ U calculations, variation of moments with U values, simulated heat capacity, and further discussions on XRD refinement.
- [78] M. Cococcioni and S. de Gironcoli, *Phys. Rev. B* **71**, 035105 (2005).